

Implementation and experimental validation of surface electromyogram and force model of Tibialis Anterior muscle for examining muscular factors

Proc IMechE Part H:
J Engineering in Medicine
1–10

© IMechE 2019

Article reuse guidelines:

sagepub.com/journals-permissions

DOI: 10.1177/0954411919890150

journals.sagepub.com/home/pih



Sridhar P Arjunan¹ , Ariba Siddiqi², Ramakrishnan Swaminathan³ 
and Dinesh K Kumar¹

Abstract

This study reports a surface electromyogram and force of contraction model. The objective was to investigate the effect of changes in the size, type and number of motor units in the Tibialis Anterior muscle to surface electromyogram and force of dorsiflexion. A computational model to simulate surface electromyogram and associated force of contraction by the Tibialis Anterior muscle was developed. This model was simulated for isometric dorsiflexion, and comparative experiments were conducted for validation. Repeated simulations were performed to investigate the different parameters and evaluate inter-experimental variability. An equivalence statistical test and the Bland–Altman method were used to observe the significance between the simulated and experimental data. Simulated and experimentally recorded data had high similarity for the three measures: maximal power of power spectral density ($p < 0.0001$), root mean square of surface electromyogram ($p < 0.0001$) and force recorded at the footplate ($p < 0.03$). Inter-subject variability in the experimental results was in-line with the variability in the repeated simulation results. This experimentally validated computational model for the surface electromyogram and force of the Tibialis Anterior muscle is significant as it allows the examination of three important muscular factors associated with ageing and disease: size, fibre type and number of motor units.

Keywords

Surface electromyography, electromyogram model, Tibialis Anterior muscle, simulation, force, muscular factors

Date received: 22 May 2019; accepted: 29 October 2019

Introduction

Surface electromyogram (sEMG) is the recording of the electrical activity of a muscle non-invasively, which is induced on the surface due to the superposition of the action potentials (APs) generated by motor units (MUs) in the muscle (motor unit action potential (MUAP)).^{1–4} Studies have shown the changes in the neuromuscular parameters that influence the signal. However, this is not well understood because the signal is influenced by multiple parameters: activation rate, conduction velocity, size and type of MUs and tissue properties.^{5–7} The relationship of muscle properties and sEMG features has only been heuristically investigated.^{1,8,9}

Research studies^{10–14} have reported various computational sEMG models to understand the changes in sEMG due to neuromuscular parameters. While the earlier models provide conceptual and generic explanation of the signal, some of the approximations that have

limited their suitability for investigating age- or disease-associated changes are as follows:

1. *Statistical distribution*: the reported models have allocated single values to their input parameters and have not considered the characteristic variability. The models reported by Farina et al.¹⁵ and Mesin et al.¹⁶ applied a normal distribution for conduction velocity.

¹SRM Institute of Science and Technology, Chennai, India

²Biosignals Lab, School of Engineering, RMIT University, Melbourne, VIC, Australia

³Indian Institute of Technology Madras, Chennai, India

Corresponding author:

Sridhar P Arjunan, SRM Institute of Science and Technology, 603203 Chennai, Tamil Nadu, India.

Email: sridhar_arjunan@ieee.org

2. *Number and size of MU*: apart from Arjunan et al.⁴ and Mesin et al.,¹⁶ the earlier models have not considered the change in number and size of MUs. This limits the investigation in the neuromuscular changes of MUs.
3. *Types of fibre*: the ratio of Type II (fast) and Type I (slow) fibre is an important neuromuscular parameter that needs to be monitored.¹⁷

Earlier models^{12–14} have represented generic parallel fibre muscles for the generation of sEMG, making them unsuitable for studying pennate muscles (e.g. Tibialis Anterior (TA)). Investigating TA is vital for determining posture stability and gait assessment.¹⁸ Even though recent modelling work^{13,16,19–21} has reported using volume conductor models to the architecture of the pennate muscle, they are inadequate due to the previous limitations listed.

Validating computational models of the complex biological system requires comparison of simulated with experimental data.²² In the case of neuromuscular experiments, the inputs are not under the direct control of the examiner because of the voluntary control by the subject, reflexive component and other factors. It is not credible to validate such a model with a single output such as sEMG but should require two or more outputs. To overcome this shortcoming, models that simultaneously simulate force and sEMG have been previously investigated.^{23,24} However, these studies have made an assumption that does not represent the physiology of the neuromuscular system; single force output of the muscle, whereas in reality there is an integration of individual muscle fibre twitch force. This limits the model ability to investigate factors such as effect of muscle fibre type on force and sEMG.

This study reports an improved computational model for simulating the force and the sEMG generated by a muscle which overcomes the shortcomings of the earlier sEMG models. It has been customized for unipennate TA under isometric conditions and been validated by comparing the features of experimentally recorded and simulated sEMG. The model was similarly validated for the force of TA during dorsiflexion (DF).

The main significances of this model are twitch force integration with precise parameters instead of arbitrary units, incorporation of joint model of ankle for computation of force and allocation of statistically distributed values to its parameters for better representation of variability due to innate biological conditions and to differentiate between the two MU types.

Materials and methods

Description of sEMG model

The model described in this study is an adaptation from the sEMG model of biceps brachii.⁴ It incorporates the

following from the earlier model:⁴ statistical distribution of parameters,²⁵ difference between fibre type, non-linear MU recruitment^{25–27} and various sizes of MUs.^{27,28} The significance of this model is that it has added the following three new features: *twitch force*, *pennation angle* and *single fibre action potential* (SFAP).

SFAP. The biceps brachii sEMG model described by Arjunan et al.⁴ and other models^{12–14,21} simulated a constant shape to explain the MUAP at the fibre level. This prevents the user to investigate the generation and extinction of the AP and the effect of inter-electrode distance as it travels.⁴ Although this is valid for the parallel muscle fibres (biceps), this makes it unsuitable for pennate muscles (TA).¹⁶ To overcome this limitation, it is necessary to generate sEMG based on SFAP.

An AP propagates along the excited motor neuron's fibre, eventually arriving at the neuromuscular junction where the motor neuron attaches to its muscle fibres. The intracellular AP recorded by an electrode from a single fibre is known as an SFAP. Collectively, these SFAPs create the MUAP.

In order to model the generation of the SFAP, Dimitrov and Dimitrova²⁹ used equation (1) and based on our earlier biceps brachii sEMG model, this was modelled for a fusiform muscle as the volume conductor.⁴ However, this was improved for the depth-inclined pennate TA.

In our model, the following values were used as reported in the literature:^{11,30}

- (a) Intracellular conductivity = 1.01 S mm^{-1} .³⁰
- (b) Extracellular conductivity = 0.089 S mm^{-1} .¹¹
- (c) The axial conductivity = 0.33 S mm^{-1} and radial conductivity = 0.0633 S mm^{-1} for the anisotropy.³⁰

Pennation angle. Researchers have developed the numerical solutions for volume conduction model of bipennate muscles.^{20,21} However, these are computationally very complex. In a bipennate muscle, the conductivity tensor becomes inhomogeneous as it changes its directions between the unipennate halves.¹³

Surface electrode recordings are largely unaffected by distant sources and thus the deeper part of the bipennate muscle¹⁶ would not significantly contribute to them. This justifies the approximation that an unipennate model can be used for TA and enables for an analytical volume conductor solution.

The volume conductor function for a muscle fibre is expressed in equation (1)

$$ft = \frac{\partial}{\partial z} \left(\frac{\sigma_i}{4\pi\sigma_e \sqrt{(z_o - z_{NMJ} \pm z') \cdot \cos \theta)^2 + K_{an} [(x_o - x_{NMJ})^2 + (y_o - y_{NMJ} \pm z' \cdot \sin \theta)^2]} \right) \quad (1)$$

Table 1. Parameters used for simulation of Tibialis Anterior sEMG and force.

Model parameter	Values reported in the literature	Values for 'Young' Tibialis Anterior simulation – variations to model inter-subject variability
Number of motor units	125–652 ³² 192 + 5 ⁴⁷ 150 + 43 ⁴⁴ 129 ³⁶ 445 ³⁵	100; 150; 200; 250; 300; 360; 380; 445; 652
Percentage of Type I fibres (%)	76 + 7 ³⁹ 70 ^{36,40} 72 + 6.4 ³⁸	30; 50; 70; 80; 90 ³⁶
Type I muscle fibre cross-sectional area (μm^2)	3950 + 950 ³⁹ 4830–5290 ³⁴	3950 ³⁸
Type II muscle fibre cross-sectional area (μm^2)	8070 + 1850 ³⁹ 8060–8800 ³⁴	8070 ³⁸
Fast fibres conduction velocity (m/s)	2.6–5.3 ²¹	4.9 + 0.3 ²¹
Slow fibres conduction velocity (m/s)		3.9 + 0.3
Total number of muscle fibres	96,800–162,500 fibres ⁴⁰	96,800; 131,000 fibres; ³⁹ 162,500
Innervation ratio		Poisson distribution with $\lambda = 364$
Muscle length (cm)	28.4–32.2 ⁴⁸ 30.0 + 0.8 ³⁷	29.8 ⁴³
Muscle fibre length (cm)	6.9–9.3 ⁴⁸ 4.5 + 0.4 ³⁷ 7.0 + 1.3 ⁴²	4.0; 4.5; 6.9; 7.7 ^{42,43,46,48}
Pennation angle ($^\circ$)	5 ⁴⁸ 20 + 2 ⁴² 12.1 + 2.2 ⁴⁶	0 $^\circ$; 5 $^\circ$; 10 $^\circ$; 12 $^\circ$; ⁴⁶ 20 $^\circ$; 30 $^\circ$
Duration of AP along fibre (mm)	11 ³³ 16 ⁴⁵	16 ⁴⁵
Subcutaneous tissue (mm)		Single, 3-mm isotropic layer
Slow-type specific force (N cm^{-2})	8.5 + 1.6 ³⁷	15.5 + 5.0 ⁴¹
Fast-type specific force (N cm^{-2})	13.1 + 2.0 ⁴¹	17.9 + 7.3
Tibialis Anterior tendon moment arm (cm)	4.9 + 0.06 ³⁷ 3.4 + 0.3 ⁴²	4.9 + 0.4 ⁴²
Simulation sampling frequency (Hz)		10,000

AP: action potential.

where f_t is the volume conduction function, σ_e and σ_i are the extra- and intracellular conductivities, K_{an} is the anisotropic factor, (x_o, y_o, z_o) is the location of the recording electrode, $(x_{NMJ}, y_{NMJ}, z_{NMJ})$ is the location of the neuromuscular junction and (x, y, z) is the coordinate system of the muscle fibre.³¹ θ is the degree at which the muscle fibre is inclined to the electrode. (x', y', z') indicates the position of the AP travelling the length of the fibre.

The neuromuscular parameters reported in the literature^{15,30,32–48} were used to model the sEMG and force of TA (summarized in Table 1). The variability in the recruitment pattern and the MU firing rate was modelled as described subsequently.

MU firing rate. This study has used the estimation of the firing rate of TA as reported by De Luca and Hostage⁴⁹ in equation (2). The 'onion skin' phenomenon represented by equation (2) describes: (1) the rate of discharge increases with ϕ , % of maximum voluntary contraction (MVC) and (2) higher firing rates are achieved by first recruited MUs compared to those recruited later

$$\lambda(\phi, \tau) = D \cdot \phi + \left(C - A \cdot e^{-\frac{\phi}{B}} \right) \cdot \tau + E \quad (2)$$

where λ is the MU firing rate; ϕ is the % MVC; τ is the recruitment threshold of MU; and the range of the firing rate being 8–30 Hz were used to derive the constants.⁴⁹

To simulate the variations in the firing rate, the variance was considered in a way that the coefficient of variation (CV) decreases exponentially with increasing MVC as reported by Jesunthadas et al.⁵⁰ The CV in the MU firing rate is expressed in equation (3)

$$CV = F + \left(\frac{\tau_i}{25} \right) + \left(\frac{\phi}{4} \right) \cdot e^{(-\Delta\phi)} \quad (3)$$

where ϕ is the % MVC, τ_i is the recruitment threshold of the i th MU, and F is a constant.

Recruitment pattern. We have incorporated the experimental outcomes reported by Klass et al.,²⁸ where they have determined that the younger subjects show continuous MU recruitment from 1% to 90% MVC having a skewed distribution (median = 26.3% MVC, skewness = 0.641

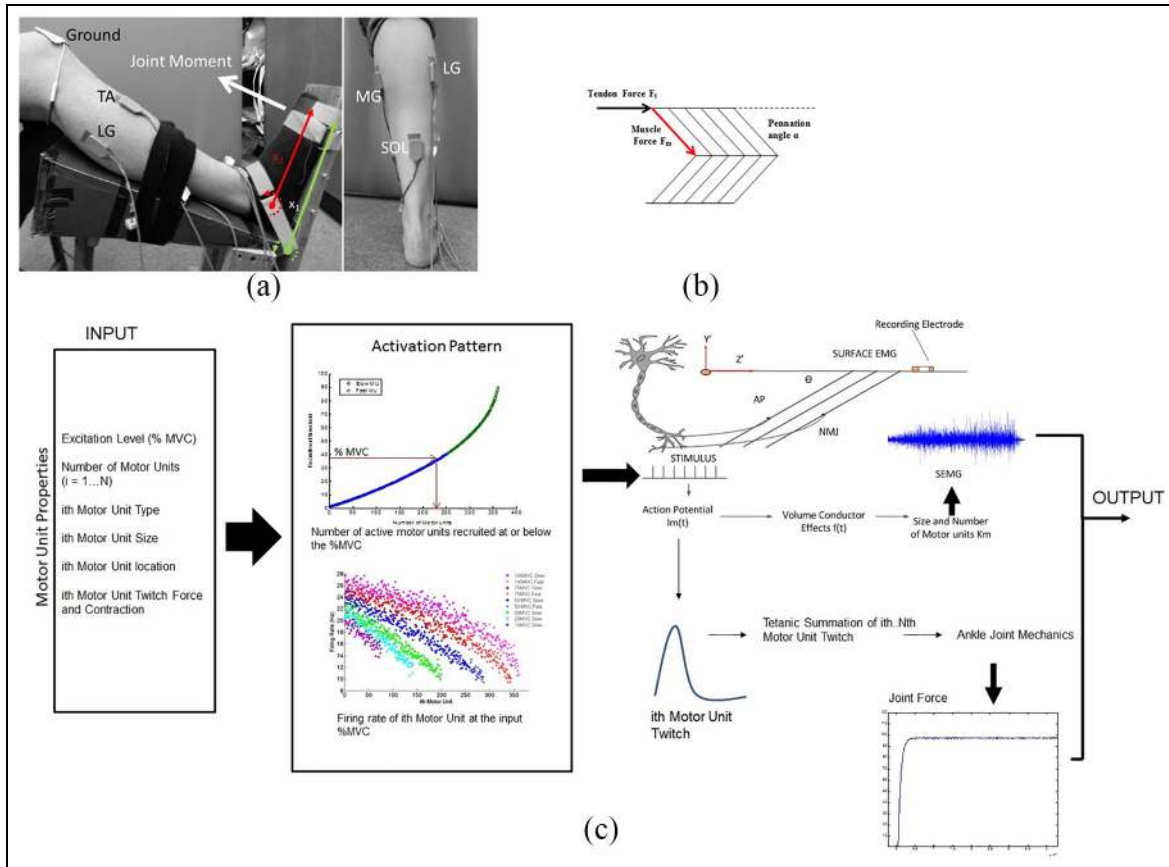


Figure 1. (a) Experimental setup and the electrode placement, (b) muscular forces, and (c) input and output of sEMG and force model.

and kurtosis = -0.491) and applied Henneman's 'size principle'.

Implementation of force model

The force model developed by Fuglevand et al.⁵¹ has been adapted in this study. However, in the original model, the peak twitch amplitude was not based on the muscle anatomical properties but was assigned arbitrary values. This may demonstrate the concept, but it is not accurate due to the varying levels of force generated by different muscle fibres. This model has overcome this limitation by computing the amplitude of the peak twitch as a function of the following three factors:^{52,53} number of muscle fibres constituting the MU, muscle fibre cross-sectional area and the type of muscle fibre.

This model has incorporated the integration of twitch force with modified contraction time of an MU to undergo a normal distribution based on the study by Van Cutsem et al.³² This study has considered Type I fibres to have twice the time of Type II fibres.⁵⁴

Computation of resultant force

It is essential to compare the experimental and simulated recordings for validating the model. As it is impossible to directly record the force of muscle contraction but only the force at a sensor placed on the

surface of the limb, the simulated muscle force needs to be transformed suitably. The first step is to convert it to tendon force and then the resultant force at the sensor using the joint moment (Figure 2(b)) based on the estimated length of insertion (Figure 1(a) and (b)). The muscle force (F_m) is first converted to the tendon force (F_t) using equation (4)

$$F_t = F_m \cdot \cos \alpha \quad (4)$$

where α is the pennation angle of the TA.

The joint moment is computed by considering the moments centred on the tibiotalar joint⁴² as expressed in equation (5)

$$\text{Jointmoment} = F_t \cdot d \quad (5)$$

where d is the tendon moment arm of the TA.

The resultant force recorded by the force sensor is obtained by considering the moments centred about the footplate hinge point (Figure 3) and is mentioned in equation (6)

$$\text{Resultantforce} = \frac{\text{Jointmoment} \cdot x_1}{x_2} \quad (6)$$

where x_1 and x_2 are the distances between the first interphalangeal joint of the foot and hinge point at the footplate and the tibiotalar joint, respectively.

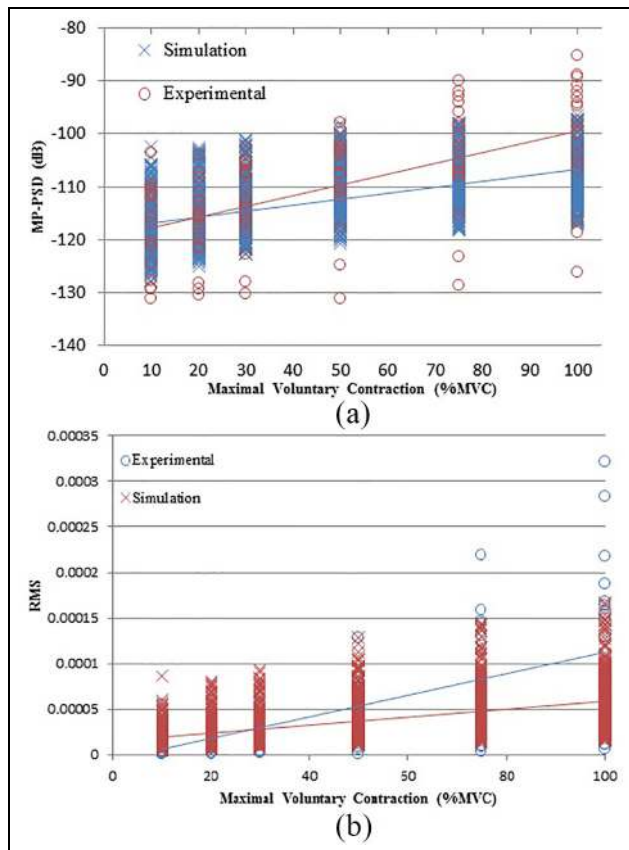


Figure 2. Scatter plot with line of best fit for (a) MP_PSD and (b) RMS of the simulated and experimental sEMG with change in percentage MVC.

An overview of the implementation and the process of sEMG and force model are illustrated in Figure 1. The MUs have a specific activation pattern, which has been used to produce the stimulus. It represents the neural impulses travelling down from the central nervous system (CNS). This initiates a train of APs to generate the MU twitch, which in turn leads to a muscular contraction through the excitation and contraction process.⁵⁵

Experimental procedures

The experimental procedures used in this study have been reported in our earlier studies.^{31,26,56}

Experimental protocol. This study protocol was approved by the 'RMIT University Human Research Ethics Committee' (SEHAPP 15751 (40/13)) and was carried out in accordance with the Declaration of Helsinki. All subjects gave written informed consent before the start of the experiments and sEMG recordings. Eighteen young healthy volunteers (9 males and 9 females; 26.1 ± 2.9 years; 166.7 ± 8.9 cm; body mass index (BMI): 22.3 ± 2.9) participated in the experiments.

sEMG was recorded from the TA and Triceps Surae (TS) muscles using the Delsys myomonitor 4

(DELSYS, Boston, USA) system, having gain of 1000 and bandwidth of 20–450 Hz. The contacts in electrodes ($10 \text{ mm} \times 1 \text{ mm}$) have a fixed inter-electrode distance of 10 mm, with the preamplifier embedded on the electrode. The sampling frequency was set at 1000 Hz with a resolution of 16 bits/sample. The electrodes were placed on the recommended locations⁵⁷ as shown in Figure 2(a).

Recording of force data. The volunteers were seated in a chair with hip flexed at 90° , knee at 140° and ankle at 90° . To prevent any foot or toe movement and heel lift, the foot and ankle were strapped to the footplate.⁵⁶ The force produced by the ankle was measured by using an S-type force transducer (SM-100 type; INTERFACE, Arizona, USA) attached to the footplate.

The volunteers performed a training session to produce their true MVC during both isometric DF and before the experiments. They were provided visual feedback of the force sensor output and given verbal encouragement. The volunteers repeated the MVC trials until their consecutive force recordings differed less than 5%. After a period of 15-min rest, the volunteers performed isometric DF at 10%, 20%, 30%, 50%, 75% and 100% MVC in a software-generated random order. Each contraction was for 5 s and was repeated twice with a 2-min rest between each trial.³¹ The antagonist force produced by the TS was quantified based on its sEMG–force relationship, which was identified during plantarflexion (PF).⁵⁸

Simulation protocol

The model was simulated at 10%, 20%, 30%, 50%, 75% and 100% MVC for 6 s. This 6 s time window is long enough for steady-state force and short enough for estimating the activity close to 100% MVC.⁵⁹ As a first step, the following five anatomical parameters were fixed because these do not vary within a same person:

1. the number of MUs,
2. muscle fibres,
3. Ratio of fast to slow fibre,
4. length of fibre and
5. pennation angle.

The simulation was repeated 18 times with values of these parameters based on the ranges shown in Table 1 to consider the variability observed in the experimental sEMG. All the other parameters were obtained based on the assumption of normal distribution of the values (Table 1). A total of 108 simulations were performed.

The simulated outputs were processed based on the recording device specifications to compare simulated and experimental recordings and downsampled to 1000 Hz, mimicking the filter characteristics and sampling frequency of the experimental recording.³¹

Data analysis

SEMG data analysis. The initial and last 1 s of the experimental sEMG and force recordings were discarded because they contained transients, while this study was designed for steady state. Maximal power of the power spectral density (MP-PSD) and root mean square (RMS) were calculated for both the simulated sEMG and experimental sEMG. MP-PSD was computed using a 25% overlap with epoch lengths of 512 points.⁶⁰

Force data analysis. Determining the true force produced by TA requires the estimation of the force produced by TS as an antagonist. This was done by computing the RMS of TS at the submaximal contractions. The antagonistic force generated by TS was estimated by considering the force–sEMG relationship for the TS as reported by Baratta et al.⁵⁸ To obtain the agonist TA force, the estimated antagonistic TS force was added to the resultant DF force at each %MVC.⁶¹

Statistical analysis. To validate the computational model, the agreement between simulated and experimentally recorded EMG data was investigated using the Bland–Altman graphical method.⁶² The linearity test ($\alpha = 0.05$) using the Bland–Altman method was also performed to determine the significance of the agreement between the features (MP-PSD and RMS) of simulated and experimental sEMG.

Shapiro–Wilk test was performed to determine whether the mean and variance of the intervals follow the normal distribution. Since the data were normally distributed, a statistical equivalence test was performed to investigate whether the simulated and experimentally recorded normalized forces are close enough and lie within the equivalence margin.⁶³ In this study, the equivalence margin was defined as the range where the difference between the simulated and experimental mean data is acceptable and considered close enough to claim that the two means are equal. Statistical significance (p -value) was computed to observe the confidence interval for the difference is completely within the equivalence margin to claim the equivalence.

Results

Figure 2 shows the scatter plot for the MP-PSD and RMS of simulated and experimental sEMG to observe the linearity with the force. It is observed that MP-PSD and RMS increase with increasing force levels, with simulated data following the experimental trend and having comparable values. The range of simulated values is within the experimentally observed values.

Figure 3 shows the Bland–Altman plots for MP-PSD, RMS and normalized force measurements. From this plot, it is observed that 98% of the ratios between MP-PSD of simulated and experimental sEMG lie

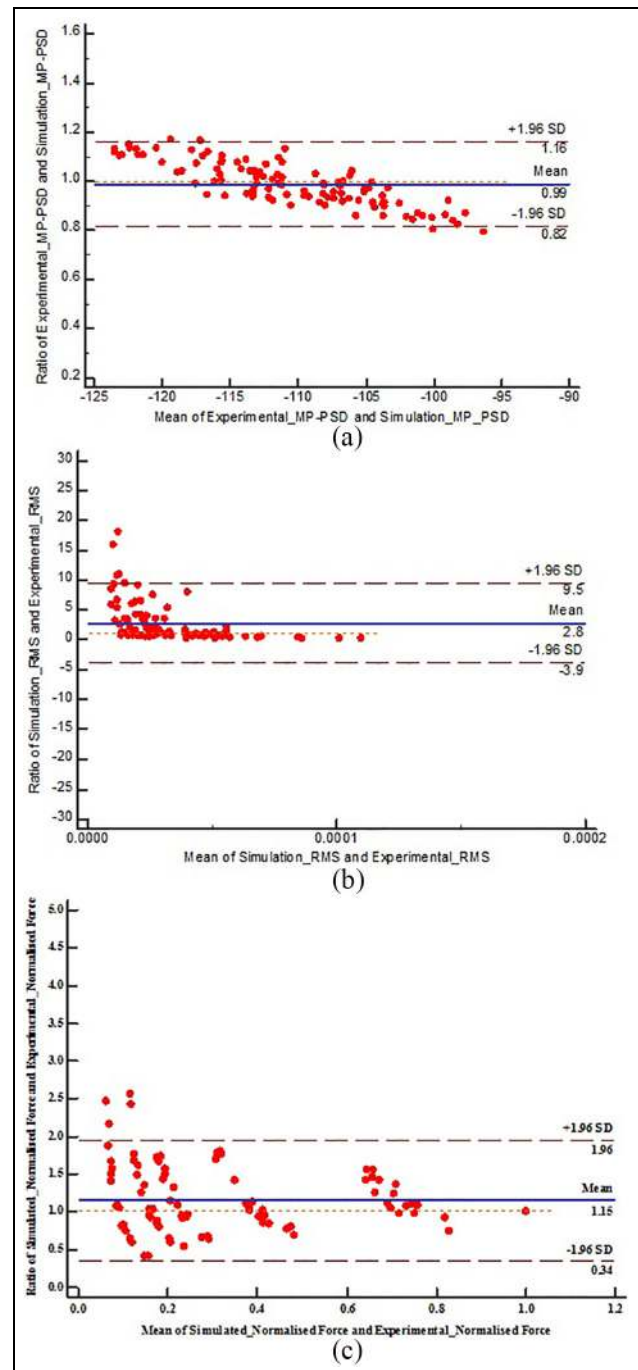


Figure 3. Bland–Altman plot to observe the agreement between the features of experimental and simulated sEMG and the force (a) MP-PSD, (b) RMS and (c) normalized force.

within the upper and lower limits of 1.96 standard deviation (SD), and this confirms agreement. This is also confirmed by the significance of the linearity test ($p < 0.0001$) using the Bland–Altman method.

It is also observed that 95% of the ratios between the RMS measured from simulated and experimental sEMG lie within the upper and lower limits of 1.96 SD and confirms the agreement between simulated and experimental sEMG. This is confirmed by the significance of the linearity test ($p < 0.0001$) using the Bland–Altman method.

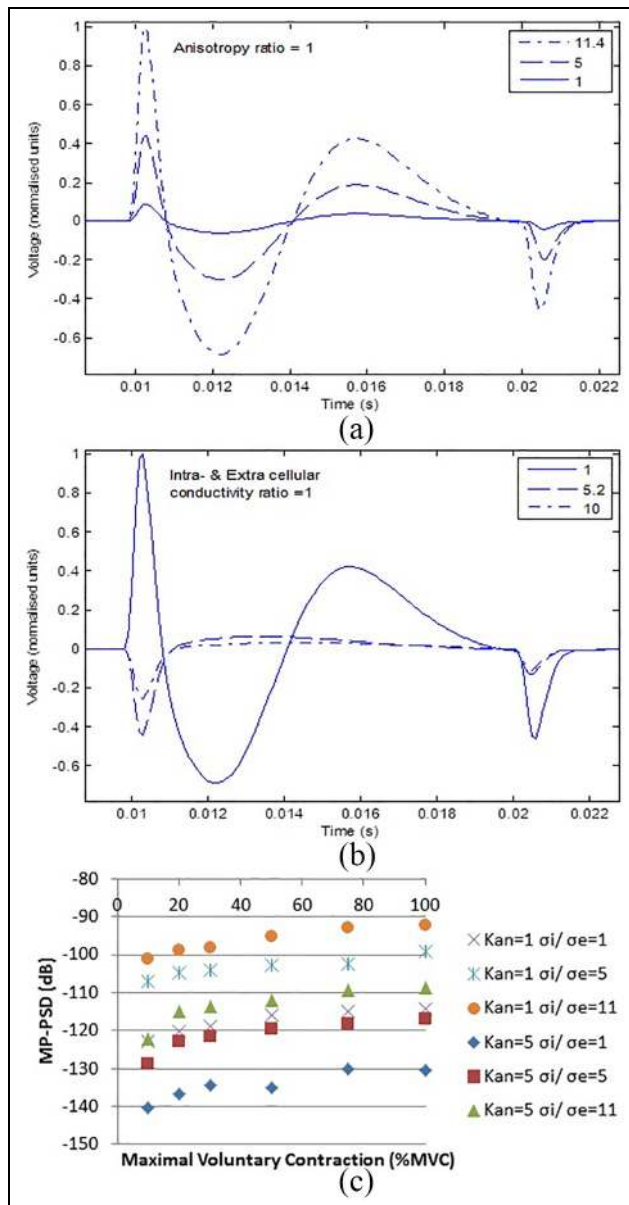


Figure 4. (a) Effect of different extracellular and intracellular conductivity ratios on the SFAP, (b) effect of anisotropic ratios on the SFAP and (c) effect of different extracellular and intracellular conductivity ratios and anisotropic ratio on the MP-PSD.

Similarly, 96% of the ratios between the normalized force sensor measurements from simulated and experimental sEMG lie within the upper and lower limits of 1.96 SD. This confirms that the simulated and experimental normalized measurements agree with each other. A test of equivalence shows that the equivalence margin values lie within 95% confidence interval to claim the equivalence with the significance p -value of 0.03.

Discussion

This article has explained and validated an sEMG model of TA and resultant force measured at the

footplate during ankle DF. This model has included the details of the neuromuscular parameters: variations in Type I and Type II fibres, the non-linearity of MU recruitment, integration of individual muscle fibre twitch force and number and size of MUs.

The feature of both the simulated and experimental sEMG linearly increase with %MVC and was statistically significant based on the linearity test performed using the Bland–Altman method. The simulated and experimental values lie within the upper and lower limits of 1.96 SD and hence confirms the agreement between the measurements. The results show that the inter-subject variability was higher in the experimental data compared with the simulated data despite the simulated parameters being randomly obtained from the corresponding range.

Table 1 shows the various ranges of values for each parameter reported in the literature. It shows that there is a very high level of variability, such as the number of MUs reported being in the range from 125 to 652.^{32,35,44} Similarly, the muscle fibres in the TA reported varied from 96,000 to 162,000.³⁸ There are also large variabilities in the values of intra- (σ_i) and extracellular conductivity (σ_e) and the anisotropy ratio of the muscles (K_{an}),^{30,64,65} which suggests that there is large inter-subject variability in the parameters. However, this may not be observable in the simulation when considering only 18 subjects because of the number of parameters being large.

Further simulations were conducted to investigate the effect of the intracellular and extracellular conductivities. The results show that the extracellular and intracellular conductivity ratios influence the SFAP's amplitude as shown in Figure 4(a). From Figure 4(b), it is also observed that the anisotropy affects both its amplitude and wave shape⁶⁶ and the amplitude of the AP decreases with an increase in anisotropy and 'stretch' its shape of the wave, which shows high variability. This condition was simulated and the effect of different extracellular and intracellular conductivity ratios and anisotropic ratios on the MP-PSD is shown in Figure 4(c).

Modelling is a simplified representation of a real-world application, and in the process, a few assumptions are made. In this study, the volume conductor of TA is modelled as unipennate instead of bipennate. The validity of this assumption is based on the deeper fibres having very small impact on the measurements from the surface.

Also, the computation of the simulated resultant force at the footplate assumes that the ankle is two-dimensional (2D) and disregards any difference in the moment arms x_1 and x_2 shown in equation (6). This assumption is reasonable for isometric contraction but limits generalization. While more natural representations of volume conductor have been reported,^{13,19,21} in this study we have investigated the model only for isometric contractions due to the limits in the assumptions.^{12,25,27,29}

Another significant inference is that the shortening of muscle fibres can impact the Median Frequency (MDF)²⁷ and could explain the reduced variability in the simulated compared with experimental sEMG. It has been shown that pennate muscles can still undergo a decrease in fibre length and increased pennation angle under isometric contraction.^{28,46}

Future work could investigate the detailed volume conductor representation to consider change in length. The ankle model that has been used to compute the resultant force from the generated muscle force is represented as 2D with fixed moment arms. It has also been assumed that it is a point load rather than a distribution on the footplate. These assumptions could be the cause of the difference between experimental and simulated force measurements. Another assumption in this study is that only TA has been considered while it is one of the four muscles that is responsible for ankle DF.⁶⁷

Conclusion

A computational model of sEMG and force signal for TA muscle that describes the sEMG recorded using differential electrodes and the resultant force measured on the footplate has been reported. The model has included physiological details that have not been described in previous models: muscle fibre type, number of muscle fibres, differential surface electrodes, pennation angle and twitch force of each MU. It has been simulated using a range of values obtained from the literature and covers the inter-subject variability. This improved model can be used to investigate changes in the TA muscle based on sEMG and force generated at the footplate during isometric DF. This would be developed to study the changes in neuromuscular parameters that cannot be estimated directly such as number, size and type of MUs. It can provide the adaptability to study the effect of ageing and decline in strength due to various muscular factors.

Acknowledgements

The authors would like to acknowledge that this manuscript includes information reported in the PhD dissertation by AS. The thesis can be accessed online and that the publication of its content is in line with the author's university policy. The part of the work by SPA was supported by Science Engineering Research Board (SERB), India, under the TARE scheme.

Author Contributions

AS, SPA, RS and DKK conceived the theoretical framework. AS and DKK designed the model. AS and SPA performed numerical simulations and

mathematical analysis. AS, SPA and DKK wrote the paper. AS, SPA, RS and DKK edited the manuscript.

Declaration of conflicting interests

The author(s) declared no potential conflicts of interest with respect to the research, authorship and/or publication of this article.

Funding

The author(s) received no financial support for the research, authorship and/or publication of this article.

ORCID iDs

Sridhar P Arjunan  <https://orcid.org/0000-0002-7288-0380>

Ramakrishnan Swaminathan  <https://orcid.org/0000-0002-4471-9629>

References

1. Arjunan SP and Kumar DK. Age-associated changes in muscle activity during isometric contraction. *Muscle Nerve* 2013; 47(4): 545–549.
2. Deschenes MR. Effects of aging on muscle fibre type and size. *Sports Med* 2004; 34(12): 809–824.
3. Doherty TJ, Vandervoort AA and Brown WF. Effects of ageing on the motor unit: a brief review. *Can J Appl Physiol* 1993; 18(4): 331–358.
4. Arjunan SP, Kumar DK, Wheeler K, et al. Effect of number of motor units and muscle fibre type on surface electromyogram. *Med Biol Eng Comput* 2016; 54(4): 575–582.
5. Farina D, Cescon C and Merletti R. Influence of anatomical, physical, and detection-system parameters on surface EMG. *Biolog Cybernet* 2002; 86(6): 445–456.
6. Farina D, Merletti R and Enoka RM. The extraction of neural strategies from the surface EMG: an update. *J Appl Physiol* 2014; 117(11): 1215–1230.
7. Rodriguez-Falces J and Place N. Effects of muscle fibre shortening on the characteristics of surface motor unit potentials. *Med Biol Eng Comput* 2014; 52(2): 95–107.
8. Ertuğrul ÖF, Kaya Y and Tekin R. A novel approach for SEMG signal classification with adaptive local binary patterns. *Med Biol Eng Comput* 2016; 54(7): 1137–1146.
9. Istenič R, Kaplanis P, Pattichis C, et al. Multiscale entropy-based approach to automated surface EMG classification of neuromuscular disorders. *Med Biol Eng Comput* 2010; 48(8): 773–781.
10. Cao H, Boudaoud S, Marin F, et al. Surface EMG-force modelling for the biceps brachii and its experimental evaluation during isometric isotonic contractions. *Comp Meth Biomech Biomed Eng* 2015; 18(9): 1014–1023.
11. Disselhorst-Klug C, Silny J and Rau G. Estimation of the relationship between the noninvasively detected activity of single motor units and their characteristic pathological changes by modelling. *J Electromyogr Kinesiol* 1998; 8(5): 323–335.
12. Merletti R, Lo Conte L, Avignone E, et al. Modeling of surface myoelectric signals. I. Model implementation. *IEEE Trans Biomed Eng* 1999; 46(7): 810–820.

13. Mesin L. Simulation of surface EMG signals for a multi-layer volume conductor with triangular model of the muscle tissue. *IEEE Trans Biomed Eng* 2006; 53(11): 2177–2184.
14. Stegeman DF, Blok JH, Hermens HJ, et al. Surface EMG models: properties and applications. *J Electromyogr Kinesiol* 2000; 10(5): 313–326.
15. Farina D, Fattorini L, Felici F, et al. Nonlinear surface EMG analysis to detect changes of motor unit conduction velocity and synchronization. *J Appl Physiol* 2002; 93(5): 1753–1763.
16. Mesin L, Merletti R and Vieira TM. Insights gained into the interpretation of surface electromyograms from the gastrocnemius muscles: a simulation study. *J Biomech* 2011; 44(6): 1096–1103.
17. Rowan SL, Rygiel K, Purves-Smith FM, et al. Denervation causes fiber atrophy and myosin heavy chain co-expression in senescent skeletal muscle. *PLoS ONE* 2012; 7(1): e29082.
18. Moreland JD, Richardson JA, Goldsmith CH, et al. Muscle weakness and falls in older adults: a systematic review and meta-analysis. *J Am Geriatr Soc* 2004; 52(7): 1121–1129.
19. Farina D, Mesin L and Martina S. Advances in surface electromyographic signal simulation with analytical and numerical descriptions of the volume conductor. *Med Biol Eng Comp* 2004; 42(4): 467–476.
20. Mesin L. Volume conductor models in surface electromyography: computational techniques. *Comp Biol Med* 2013; 43(7): 942–952.
21. Mesin L and Farina D. Simulation of surface EMG signals generated by muscle tissues with inhomogeneity due to fiber pinnation. *IEEE Trans Biomed Eng* 2004; 51(9): 1521–1529.
22. Sargent GR. Verification and validation of simulation models. *J Simulat* 2013; 7(1): 12–24.
23. Hashemi J, Morin E, Mousavi P, et al. Surface EMG force modeling with joint angle based calibration. *J Electromyogr Kinesiol* 2013; 23(2): 416–424.
24. Liu P, Liu L and Clancy EA. Influence of joint angle on EMG-torque model during constant-posture, torque-varying contractions. *IEEE Trans Neural Syst Rehabil Eng* 2015; 23(6): 1039–1046.
25. Wheeler K, Kumar D, Shimada H, et al. Implementing a surface EMG model with accurate parameters and a force output. In: *ISSNIP biosignals and biorobotics conference*, Vitoria, Brazil, 6–8 January 2011, pp.1–5. New York: *IEEE*.
26. Siddiqi A, Kumar D, Arjunan SP, et al. A model for generating Surface EMG signal of m. Tibialis Anterior. In: *2014 36th annual international conference of the IEEE engineering in medicine and biology society*, Chicago, IL, 26–30 August 2014, pp.106–109. New York: *IEEE*.
27. Maitra Ghosh D, Kumar D, Poosapadi Arjunan S, et al. A computational model to investigate the effect of pennation angle on surface electromyogram of Tibialis Anterior. *PLoS ONE* 2017; 12(12): e0189036.
28. Klass M, Baudry S and Duchateau J. Age-related decline in rate of torque development is accompanied by lower maximal motor unit discharge frequency during fast contractions. *J Appl Physiol* 2008; 104(3): 739–746.
29. Dimitrov GV and Dimitrova NA. Precise and fast calculation of the motor unit potentials detected by a point and rectangular plate electrode. *Med Eng Phys* 1998; 20(5): 374–381.
30. Lowery MM, Vaughan CL, Nolan PJ, et al. Spectral compression of the electromyographic signal due to decreasing muscle fiber conduction velocity. *IEEE Trans Rehabil Eng* 2000; 8(3): 353–361.
31. Siddiqi AM. *Relative contributions of neuromuscular factors to muscle strength decline with age*. Melbourne, VIC, Australia: RMIT University, 2016.
32. Van Cutsem M, Feiereisen P, Duchateau J, et al. Mechanical properties and behaviour of motor units in the Tibialis Anterior during voluntary contractions. *Can J Appl Physiol* 1997; 22(6): 585–597.
33. Dumitru D, King JC and Rogers WE. Motor unit action potential components and physiologic duration. *Muscle Nerve* 1999; 22(6): 733–741.
34. Edstrom L and Nystrom B. Histochemical types and sizes of fibres in normal human muscles. *Acta Neurol Scand* 1969; 45(3): 257–269.
35. Feinstein B, Lindegård B, Nyman E, et al. Morphologic studies of motor units in normal human muscles. *Cells Tissues Organs* 1955; 23(2): 127–142.
36. Fling BW, Knight CA and Kamen G. Relationships between motor unit size and recruitment threshold in older adults: implications for size principle. *Experiment Brain Res* 2009; 197(2): 125–133.
37. Fukunaga T, Roy R, Shellock F, et al. Specific tension of human plantar flexors and dorsiflexors. *J Appl Physiol* 1996; 80(1): 158–165.
38. Henriksson-Larsén KB, Lexell J and Sjöström M. Distribution of different fibre types in human skeletal muscles. I. Method for the preparation and analysis of cross-sections of whole tibialis anterior. *Histochem J* 1983; 15(2): 167–178.
39. Jakobsson F, Borg K, Edström L, et al. Use of motor units in relation to muscle fiber type and size in man. *Muscle Nerve* 1988; 11(12): 1211–1218.
40. Johnson MA, Polgar J, Weightman D, et al. Data on the distribution of fibre types in thirty-six human muscles: an autopsy study. *J Neurol Sci* 1973; 18(1): 111–129.
41. Krivickas LS, Dorer DJ, Ochala J, et al. Relationship between force and size in human single muscle fibres. *Experiment Physiol* 2011; 96(5): 539–547.
42. Maganaris CN. Force-length characteristics of in vivo human skeletal muscle. *Acta Physiol Scand* 2001; 172(4): 279–285.
43. Maganaris CN, Baltzopoulos V, Ball D, et al. In vivo specific tension of human skeletal muscle. *J Appl Physiol* 2001; 90(3): 865–872.
44. McNeil CJ, Doherty TJ, Stashuk DW, et al. Motor unit number estimates in the tibialis anterior muscle of young, old, and very old men. *Muscle Nerve* 2005; 31(4): 461–467.
45. Morse CI, Thom JM, Reeves ND, et al. In vivo physiological cross-sectional area and specific force are reduced in the gastrocnemius of elderly men. *J Appl Physiol* 2005; 99(3): 1050–1055.
46. Simoneau EM, Longo S, Seynnes OR, et al. Human muscle fascicle behavior in agonist and antagonist isometric contractions. *Muscle Nerve* 2012; 45(1): 92–99.
47. Trojaborg W, Kaufmann P and Gooch CL. Motor unit estimate number in the anterior tibial muscle: normative data versus findings in critically ill patients in intensive care units. *J Clin Neuromusc Dis* 2002; 3(4): 139–142.

48. Wickiewicz TL, Roy RR, Powell PL, et al. Muscle architecture of the human lower limb. *Clin Orthopaed Relat Res* 1983; 179: 275–283.
49. De Luca CJ and Hostage EC. Relationship between firing rate and recruitment threshold of motoneurons in voluntary isometric contractions. *J Neurophysiol* 2010; 104(2): 1034–1046.
50. Jesunathadas M, Klass M, Duchateau J, et al. Discharge properties of motor units during steady isometric contractions performed with the dorsiflexor muscles. *J Appl Physiol* 2012; 112(11): 1897–1905.
51. Fuglevand AJ, Winter DA and Patla AE. Models of recruitment and rate coding organization in motor-unit pools. *J Neurophysiol* 1993; 70(6): 2470–2488.
52. Narici M, Landoni L and Minetti A. Assessment of human knee extensor muscles stress from in vivo physiological cross-sectional area and strength measurements. *Eur J Appl Physiol Occupat Physiol* 1992; 65(5): 438–444.
53. Sacks RD and Roy RR. Architecture of the hind limb muscles of cats: functional significance. *J Morphol* 1982; 173(2): 185–195.
54. Maffioletti NA, Aagaard P, Blazevich AJ, et al. Rate of force development: physiological and methodological considerations. *Eur J Appl Physiol* 2016; 116(6): 1091–1116.
55. Fauler M, Jurkat-Rott K and Lehmann-Horn F. Membrane excitability and excitation–contraction uncoupling in muscle fatigue. *Neuromusc Disord* 2012; 22: S162–S167.
56. Siddiqi A, Arjunan SP and Kumar D. Improvement of isometric dorsiflexion protocol for assessment of Tibialis Anterior muscle strength. *MethodsX* 2015; 2: 107–111.
57. SENIAM. Surface electromyography for the non invasive assessment of muscles, 2009, <http://seniam.org/>
58. Baratta R, Solomonow M, Zhou B, et al. Muscular coactivation: the role of the antagonist musculature in maintaining knee stability. *Am J Sports Med* 1988; 16(2): 113–122.
59. Hogrel JY, Duchêne J and Marini JF. Variability of some SEMG parameter estimates with electrode location. *J Electromyogr Kinesiol* 1998; 8(5): 305–315.
60. Inbar G, Paiss O, Allin J, et al. Monitoring surface EMG spectral changes by the zero crossing rate. *Med Biol Eng Comput* 1986; 24(1): 10–18.
61. Billot M, Simoneau E, Van Hoecke J, et al. Coactivation at the ankle joint is not sufficient to estimate agonist and antagonist mechanical contribution. *Muscle Nerve* 2010; 41(4): 511–518.
62. Giavarina D. Understanding Bland Altman analysis. *Biochem Med* 2015; 25(2): 141–151.
63. Walker E and Nowacki AS. Understanding equivalence and noninferiority testing. *J Gen Intern Med* 2011; 26(2): 192–196.
64. Röhrle O, Davidson JB and Pullan AJ. A physiologically based, multi-scale model of skeletal muscle structure and function. *Front Physiol* 2012; 3: 358.
65. Van Veen BK, Wolters H, Wallinga W, et al. The bioelectrical source in computing single muscle fiber action potentials. *Biophys J* 1993; 64(5): 1492–1498.
66. Nandedkar SD and Stalberg E. Simulation of single muscle fibre action potentials. *Med Biol Eng Comput* 1983; 21: 158–165.
67. Marsh E, Sale D, McComas A, Quinlan J. Influence of joint position on ankle dorsiflexion in humans. *Journal of Applied Physiology* 1981 51(1): 160–7.